



Induced touch voltage in wayside cables of AC railways caused by traction supply transients

Jacopo Bongiorno¹

Received: 24 April 2022 / Accepted: 2 September 2022 / Published online: 19 September 2022
© The Author(s), under exclusive licence to Springer-Verlag GmbH Germany, part of Springer Nature 2022

Abstract

Many communication and signaling systems still rely on cables routed trackside and are thus exposed to induction. The evaluation of induced voltage as touch voltage and as coupled interference is particularly relevant for safety assessment, in terms of electrical and functional safety, and in general for system availability. Induction may be estimated by simplified and conservative closed-form expressions or with more complex simulation models; available models are in general developed for frequency domain. The proposed method provides accurate induced voltage waveform with moderate complexity, as caused by AC traction supply major transients for both 1×25 (no autotransformer) and 2×25 (with autotransformer) configurations. The method can use simulated or measured frequency responses followed by fitting of a polynomial transfer function $H(s)$ with good approximation (about 3–6%) over an extended frequency interval (up to 1000 Hz). Input to $H(s)$ are the transient waveforms, namely for short circuit and inrush phenomena. For short circuit the proposed calculation method is that of an equivalent circuit including all relevant elements, confronted to standardized method of EN 60909-0 for what regards peak and steady state value and time constant. The $H(s)$ output is the transient induced voltage waveform: comparing the intensity for 1×25 and 2×25 cases achieves a first validation by comparing to reduction factors documented in the literature. The method is validated using measured inrush current and resulting cable voltage, showing an average error of 2–3%.

Keywords Induction · Inrush current · Model validation · Railways · Short-circuit current · Transfer function

1 Introduction

Modern transportation systems rely on a wide range of signaling and communication systems, not only to ensure a high level of safety and performance, but also in relation to services of messaging, announcement, coordination [1, 2].

One type of devices comprises those directly connected to the rails (namely track circuits [3–5]), for which the main concern is represented by overvoltages and conductive coupling of disturbance [6–9]; including in-band interference at the same operating frequencies of the said devices.

The largest share of devices and circuits (and in particular the most modern technologies) is, however, not directly connected to the track but deployed trackside. They are not all connected by radio links or fiber optic, but many still rely on copper connections, possibly over significant distances [3,

10]. Such connections, used for supply an data, are exposed to induction caused by the traction supply current flowing in the catenary (or third rail), the running rails and all other conductors of the traction supply circuit (e.g., negative feeder, NF, for Autotransformer, AT, systems; additional return conductors, including Booster Transformer (BT) systems; backup conductors for intermediate feeding) [11].

The problem of induction is known to occur over a broad range of frequencies from the supply frequency (e.g., 16.7 Hz, 50 Hz or 60 Hz) to some kHz, above which power system harmonics decrease to less significant amplitude values [11]. Induction affects the most exposed trackside cables, lying in cable ducts next to the rails, in cable trays along walls of e.g., viaducts and tunnels, and causes induced voltages to appear across both the external shield and internal conductors. The consequences are:

✉ Jacopo Bongiorno
jacopo.bongiorno87@gmail.com

¹ RINA Services, s.r.l Via Renata Bianchi 44L, Genova 16152, Italy

- (1) the cable and connected equipment are subject to a voltage change named “touch voltage,” whenever the part is accessible to a person (worker, passenger, ...) and there is risk of electrocution (electrical safety hazard);
- (2) the voltage change is coupled on the inner signal conductors causing possible interference, as well as leakage to other parts of the connected equipment (functional safety hazard).

As a safety assessment problem, it requires that reliable and assessed tools are used, within a process that can be verified and is based as far as possible on standards, standardized procedures and easily accessible scientific literature: from this the relevance of simple, yet accurate, methods as the one proposed here.

The problem of induction may be addressed during design by means of either simulation tools or calculations with closed-form expressions, with various degrees of accuracy and confidence, in general using a pure frequency domain approach [13]. Simulation tools are possibly more configurable and accurate but require a substantial effort of comprehensive modeling of several km of line and a detailed knowledge of system electrical parameters [14, 15]. Closed-form expressions were discussed and evaluated in [13] and found enough accurate in practical cases, necessitating a reduced set of parameters.

To this framework of induction assessment, however, one important aspect still needs to be added: the evaluation of induction not for steady electrical phenomena that allow a pure frequency-domain approach [16, 17], but the inclusion of major traction supply transients; that require a different approach. Two major transients may be recognized: short circuit along the line and on-board transformer inrush.

Inrush occurs whenever the on-board transformer undergoes a step voltage change, such as at the pantograph rise against the live catenary, or—as customary—at the closure of the on-board circuit breaker, and during passage under a neutral section and can be modeled considering frequency ranges up to some hundred hertz [16–22]. Pantograph bounces as well can cause similar transients of lesser amplitude, together with electric arc phenomena, common to AC and DC railways [23–26]. Electric arcs feature a much wider bandwidth and together with high-order harmonics need a complete lumped or distributed parameters model to extend response to several kHz or higher, as demonstrated in [27] for DC systems.

Short-circuit events are characterized by a sudden intense flow of current in the traction supply circuit that may cause significant induction onto wayside cables for parallelism in excess of 1 km or so [13, 28, 29]. A pure time-domain approach (e.g., using a circuit simulator) is as accurate as the provided details and parameters, but is certainly time-consuming and does not provide directly the synthetic

overview of system behavior as for frequency-domain models [16, 17].

This work proposes a simplified hybrid time–frequency modeling method for the estimate of induced voltage across wayside cables, covering transients such as short-circuit and inrush waveforms. The method is described in Sect. 2 and then further detailed in the following Sects. 3 and 4 for modeling of induction in a real system and fitting between the Laplace and Fourier domains, and for the short-circuit or inrush waveform estimate, respectively. The model is then validated for two configurations 1×25 kV and 2×25 kV 50 Hz high-speed railway line (HSRL), using experimental results of inrush phenomena, that are allowed to be reproduced for testing purposes in a real system, whereas short circuits are a cause of stress for protections and tests are not allowed also for safety reasons.

2 Overall description

Traction supply transients should be addressed in principle with a pure time-domain approach. Traction supply transients are however electrical phenomena relevant up to some hundreds Hz, reflections and high-frequency phenomena can be neglected. Low-frequency characteristics of the traction circuit should be considered:

- the running rails have internal inductance undergoing a significant reduction for increasing frequency right at about the supply frequency [30, 33], reducing the overall impedance and slightly amplifying the flowing current;
- the track-to-earth conductance [34, 35] and the overall grounding of the return circuit are responsible for a change to the fraction of return current leaving the rails, that increases the area of the inducing loop [13].

Such terms can be effectively included in a multi-conductor transmission line (MTL) simulation model in frequency domain and must be transferred reliably to the time domain with the method proposed in this work.

A system is considered (sketched in Fig. 1) with an electric traction line, all its traction supply conductors (including those of the return circuit) and the victim wayside cables, for which the transient induced voltage $v(t)$ is to be determined (as caused by a major transient on the traction circuit indicated by the current $i(t)$). There is no limit to the number of victim cables, provided that there is no significant mutual effect (as for cables lying side by side). Results are provided for the case with the victim cable next to the ESS and the transient current flowing back to the ESS uniformly along its length.

A process can be outlined (as described in the flowchart of Fig. 2) to determine the induced voltage $v(t)$ starting from the

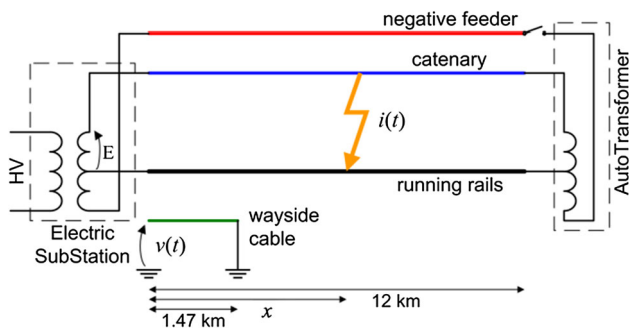


Fig. 1 Sketch of the HSRL, configurable as 1 × 25 (switches open) or 2 × 25 (switches closed); the orange flash indicates the point of discharge of the short circuit or inrush event. The considered length for the results in Sect. 5 is 12 km, victim cable is 1470 m

inducing current $i(t)$, as caused by the short-circuit or inrush current event. Characteristics of the system considered, might be provided by a simulated or a measured frequency response $T(j\omega)$, considering as input quantity the inducing current and as output the induced voltage on wayside cables. The frequency response of the system is then transformed into a transfer function (TF). The step of the procedure can be summarized as follows:

- (1) frequency-domain data are collected to describe the system by means of simulation (with the possibility of including sensitivity analysis and exploring hypothetical worst-case configurations even in the design phase) or measurements; these data consist of the frequency response vector $T(j\omega)$ used between the two identified inducing and induced quantities;
- (2) a Laplace-domain polynomial TF $H(s)$ with order n for the numerator and m for the denominator is selected, that represents a linear time invariant dynamic system that is not needed to be known;
- (3) fitting $H(s)$ onto $T(j\omega)$ is accomplished by an accepted method, such as Least Mean Square (LMS), with care to a suitable density of points on the frequency axis, especially around resonance and anti-resonance points, and using a weight vector $w(j\omega)$ to guide the fitting process; the result is $H^*(s)$;
- (4) a time-domain stimulus $i(t)$ is determined by calculation or measurements (in the following exemplified by short-circuit current see Sect. 4.1 and inrush current, Sect. 4.2);
- (5) the stimulus $i(t)$ is then applied to the system $H^*(s)$ to calculate the resulting induced voltage $v(t)$ by means of convolution with its impulse response (see Eq. (1)).

$$v(t) = \int_{-\infty}^{+\infty} i(\xi)h(t - \xi)d\xi. \tag{1}$$

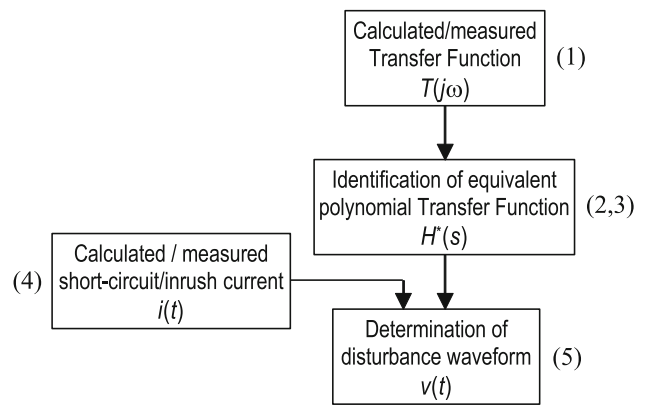


Fig. 2 Flowchart of the transient disturbance calculation process with step numbers between parentheses

It is noted that the TF describing induction is an impedance with inductive behavior, i.e., in $H(s) \ n > m$: high-frequency poles must be added to have a causal (non-anticipative) system (in general one pole is sufficient); such poles should not affect transient response and fitting, so that real poles are preferred.

3 Model of the real system

3.1 Real system model

A model of a complex system, such as a modern electric railway or metro, may be preferable to a direct approach based on measurements for the determination of TF: the real system may still be in the design phase and cannot be tested; a model allows sensitivity analysis to e.g., environmental conditions or variability of some parameters; a model allows also verifying worst cases that are not realizable in practice, but are important to ensure safety margins [14]. There must be evidence of model validation against suitable and representative experimental data [36], to ensure that the model is reliable, accurate enough, and for safety assessment ensuring no significant underestimation.

To the aim of induction calculation the model may be tailored to some representative cases, such as maximum ESS or Autotransformer (AT) separation, minimum ESS impedance for maximum short-circuit current. For the present case, for which transients all occur at the supply frequency, a low-frequency model is sufficient, e.g., accurate up to some hundreds Hz or so, for which simplified models could be used [37, 38].

The result is one or many frequency responses $T(j\omega)$, each determined for the port pair between the source injection point and the terminals across which the induced voltage is measured, defined over K points in the frequency domain, $k = 1, \dots, K$, $\omega = 2\pi f_k$. Such responses can come from mea-

Table 1 HSRL electrical and geometrical parameters for open air sections; positions provided for even and odd track with respect to the midline axis (horizontal X) and a reference plane passing through rails (vertical Y)

	Material	Resist. ($\mu\Omega$ m)	Cross section (mm^2)	pos X (m)	pos Y (m)
Negative feeder (NF)	Al	0.050	307	- 6.53	8.00
				+ 6.53	8.00
Messenger wire (MW)	Cu	0.018	120	- 2.50	6.55
				+ 2.50	6.55
Contact wire (CW)	Cu	0.018	150	- 2.50	5.30
				+ 2.50	5.30
Buried earth wire (BEW)	Cu	0.018	95	- 4.60	- 0.96
				+ 4.60	- 0.96
Overhead earth wire (OEW)	Al	0.050	150	- 6.07	5.50
				+ 6.07	5.50
Running rail (RR)	UIC60	0.225	7686	- 3.26	0.01
				- 1.74	0.01
				+ 1.74	0.01
				+ 3.26	0.01

surements or from a reliable reference simulation model. The railway system used in this paper is a high-speed line modeled with the MTL simulator described in [13] and validated among other cases in [39]. Schematic and electrical and geometrical parameters are shown in Fig. 3 and Table 1.

Slightly different conductors' arrangement may take place for other existing 2×25 kV systems: in some cases the BEW is not used and rather earthing is achieved by electrodes, whereas distributed earthing is carried out with the poles interconnected by the OEW (the so called French system). For a pure 1×25 system negative feeder is not present. In all cases a trustable and accurate simulator will output the desired $T(j\omega)$ and the proposed fitting and time-domain response calculation can be carried out.

3.2 Dynamic system identification

Electrical system identification has been extensively studied in the '90 s and more recently, for both large power networks (as in the present case) [40] and microcircuits operating at much higher frequency (with specific problems of dispersive behavior and reflections). Several approaches are possible for the identification of system response [41], either based on Auto-Regressive Moving Average (ARMA), Time-Domain Vector-Fitting (TD-VF), or Z-Domain Vector-Fitting (ZD-VF), the latter corresponding to our approach. The conclusion in [41] is that both VF methods perform better than the ARMA, and that TD-VF performs best in case of truncated time-domain signals are fed to the method (that is not our case), the ZD-VF being more robust and stable.

A Linear Time Invariant (LTI) system with TF $H(s)$ is selected. Fitting of $H(s)$ onto $T(j\omega)$ is performed by means of Least Mean Square (LMS) optimization of cost function

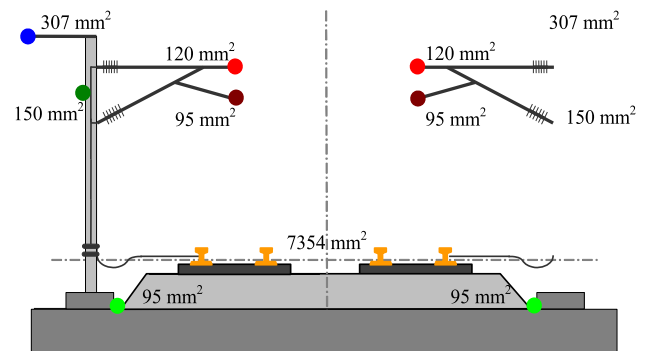


Fig. 3 HSRL cross section as implemented in the MTL model providing frequency response $T(j\omega)$; conductors as in Table 1: negative feeder (blue), messenger wire (red), contact wire (brown), overhead earth wire (dark green), buried earth wire (green), running rails (orange)

J , corresponding to the Mean Square Error (MSE), including a weight function w :

$$J = \frac{1}{K} \sum_{k=1}^K w(k) |T(j\omega(k)) - H(s = j\omega(k))|^2 \quad (2)$$

Having defined $H(s) = B(s)/A(s)$ with n zeros and m poles, (2) may be written as:

$$J = \frac{1}{K} \sum_{k=1}^K w(k) |T(k) A(k) - B(k)|^2 \quad (3)$$

The weight function can be exploited to give relevance to portions of the curve with too few points (such as at very low frequency, that is relevant for signal decay, as commented in Sect. 5.1) or to reduce the influence of resonance peaks at high frequency (necessitating too many additional poles and zeros

for adequate fitting without adding significant terms to the overall transient response). It is observed that the necessary bandwidth to reproduce short-circuit and inrush phenomena is limited to a few hundreds Hz, that should be retained in this work as the most relevant frequency interval; TF fitting is thus carried out up to 1 kHz.

Once $H^*(s)$ for the desired $i-v$ pair and system configurations are identified, the calculation of the desired output (the induced voltage) is achieved by the convolution integral in (Eq. (1)). This can be repeated for all relevant $i-v$ pairs (e.g., for different wayside cables of different injection positions along the line) and system configurations (first of all the 1×25 and 2×25 configurations and then variations of parameters).

4 Estimation of the source of induction

Two sources of induction have been identified, the short-circuit current discharging at some point along the line (named remote short circuit, to distinguish it from one occurring at substation busbar) and the inrush current flowing into the on-board transformer of an AC vehicle during initial magnetization. The latter assimilates other transients that may occur at the pantograph-to-catenary interface (pantograph bounce, passage under phase separation or neutral sections), and the port to for the excitation signal is the same.

The typical experimental approach is a direct measurement of the source of induction, the current, using a galvanically isolated probe: for the short circuit a convenient location is at the rails potential, such as at the return point back to the substation, for inrush it may be measured located e.g., on the pantograph cable or internally next to the on-board main circuit breaker. The overall measurement accuracy may be in the range of 1–2% considering modern instrumentation. This approach was followed for the validation phase using measured inrush current waveforms, as explained in Sect. 5.

An alternative approach is that of the estimation of waveforms by calculation, with which a sensitivity analysis can be carried out as well, hopefully identifying worst cases and the range of variability of waveforms parameters (e.g., peak current value and time constant of the short-circuit current while varying some of the parameters).

4.1 Short circuit current calculation

With focus on AC railways, by similarity with single-phase AC grids, the EN 60909-0 [42] could be used, that necessitates an equivalent circuit including the parameters for Autotransformers (AT), for the ESS and for the (HV) line feeding it.

Two parameters are necessary for the calculation using the EN 60909: the X/R ratio and the permanent short-circuit

Table 2 Railway system parameters for short-circuit current calculation

Substation transformer			
Primary voltage (kV)	132	Secondary voltage (kV)	27.5
Apparent power (MVA)	60	Losses %	1.0
Short-circuit react. X_{12} , $X_{13}\%$	10.5	Short-circuit react. $X_{23}\%$	10.5
Autotransformer			
Apparent power (MVA)	15	Losses %	1.0
Short-circuit reactance %	1.0		
Traction line equivalent parameters			
Resistance cat. (mΩ/m)	0.060	Resistance NF (mΩ/m)	0.077
Inductance cat. (μH/m)	0.65	Inductance NF (μH/m)	0.86
High voltage three-phase line			
Resistance (mΩ)	76	Inductance (mH)	2.4

current I_{sc} . They may be determined easily also using the equivalent circuits shown in Fig. 4, with the parameters taken from name plate data and test bulletins of the railway system components reported in Table 2. The position of the short circuit is indicated by x , variable between 0 and 1 covering the stretch of the supply section (12 km).

The reactance ratio q of the ESS transformer is defined as [41]

$$q = X_1 / (X_1 + X_2) = X_1'' / (X_1'' + X_2) \tag{4}$$

where X_1 and X_2 are the primary and secondary short-circuit reactance and the prime and double prime mean “seen from primary” and “seen from secondary”. This parameter describes how the reactance is distributed between the primary and the secondary side of the transformer and has some influence on the amplitude of the short-circuit current.

The two 25 kV secondary windings of the ESS transformer (numbered 2 and 3) can be considered identical (so that the short-circuit reactance values $X_{sc12} = X_{sc13}$).

$$X_1'' = \frac{V_2^2}{A_{n1}} (2X_{sc12} - X_{sc23}) \quad X_2 = \frac{V_2^2}{A_{n1}} X_{sc23} \tag{5}$$

The short-circuit waveform is sinusoidal (as in Fig. 1 of EN 60909-0) with peak value I_p and steady state value I_{sc} ; the maximum is attained if the sinusoidal voltage starts from zero.

$$I_p = k\sqrt{2} I_{sc} \tag{6}$$

with k given in Fig. 15 and Eq. (55) of EN 60909-0 as

$$k = 1.02 + 0.98 \exp(-3R/X) \tag{7}$$

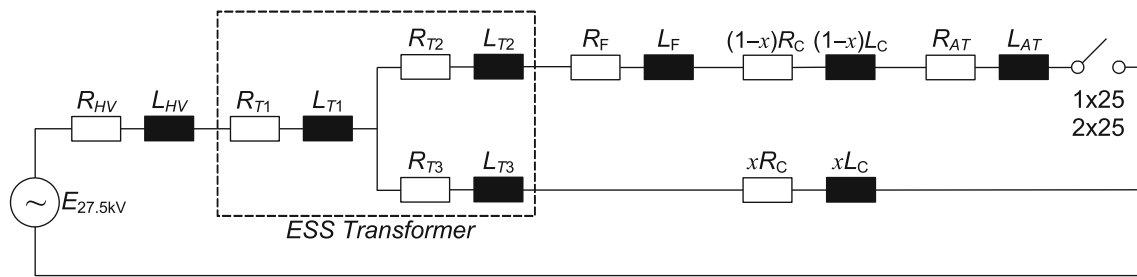


Fig. 4 Equivalent circuit of a 1×25 or 2×25 kV system for calculation of short-circuit current: the switch can exclude the AT and the system becomes a simple 1×25 network; x indicates the fractional length where the short circuit occurs. The symbols indicate: high-

voltage network upstream (HV), ESS transformer (T1, T2, T3 for the three windings), negative feeder (F), contact wire including messenger (C), autotransformer (AT)

The exponential decay is described by the quantity $I_{dc}(t)$:

$$I_{dc}(t) = \sqrt{2} I_{sc} \exp(-2\pi f t R/X) \quad (8)$$

The total short-circuit current waveform is the sum of these two components, $I_{sc}(t)$ and $I_{dc}(t)$.

For the present study the possibilities for calculation, so to include the parameters of the HV network upstream and the peculiar behavior with AT included or excluded, were performed using the same MTL simulator by positioning the short-circuit block at the desired longitudinal x value, or providing a closed-form self-evident method giving easy access to the parameters.

The latter was preferred by the design verification board and the scheme of Fig. 4 was implemented in Matlab as a LTI system itself, solving it by series and parallel manipulation of Laplace expressions for all components (code in Appendix). The EN 60909-0 was then used only as a verified reference for general information and waveform comparison.

4.2 Inrush current calculation

For the inrush phenomenon, related to the insertion of the on-board transformer onto the catenary voltage, various approaches may be used [44–46], although the preference is for analytical expressions. Three formulations (Bertagnoli, Specht and Holcomb) are discussed in [44], the latter the most accurate and providing an approximate waveform rather than the envelope of peaks only (as for the first two formulations):

$$i(t) = \frac{\sqrt{2}E}{\sqrt{R^2 + \omega^2 L^2}} \left(\sin(\omega t - \varphi) - e^{-R/L(t-t_s)} \sin(\omega t_s - \varphi) \right) \quad (9)$$

$$\varphi = \tan^{-1} \left(\frac{\omega L}{R} \right) \quad (10)$$

In general, an error up to about $\pm 40\%$ may be expected for analytical formulas, whereas numeric models [45, 46] can be more accurate, but of higher complexity and necessitate of a

larger number of parameters. To cope with the relatively large error, measured inrush waveforms are used for the validation in Sect. 5.

5 Results and validation for 1×25 and 2×25 kV 50 Hz configurations

The procedure outlined in Sect. 2 is followed for the case of a 2×25 kV high-speed line, including the case in which the AT is out of service, resulting in a simple 1×25 kV configuration. The line selected for tests is part of the Italian 2×25 kV 50 Hz high-speed network.

The short-circuit current is calculated following the method of Sect. 4.1; the inrush current waveform (discussed in Sect. 4.2) was measured and together with the measured touch voltage will be used for the validation.

5.1 Frequency response fitting

$H^*(s)$ was determined by LMS fitting of the MTL frequency responses $T(j\omega)$, as shown in Fig. 5 for the 1×25 and 2×25 cases. The frequency range is chosen extended up to 1 kHz including thus some of the first high-frequency resonances whose response is too fast to be visible in the resulting voltage waveforms for the short circuit and inrush cases. The most relevant frequency ranges are that including 50 and 100 Hz (representing the main components of short-circuit and inrush current waveforms) and the lower interval around some tens of Hz (for the short-circuit transient response over some fundamental cycles) or down to about 1 Hz (for the slower inrush transient lasting some seconds).

The two $T(j\omega)$ for the 1×25 and 2×25 configuration can be evidently approximated first with a resistive-inductive transfer function; at a closer look a staircase shape can be identified changing slope toward resistive behavior at about 10 Hz and then again inductive at about 50 Hz. The value of the $T_{1 \times 25}$ is in fact about 0.55 and 1.15 Ω at 50 and 100 Hz;

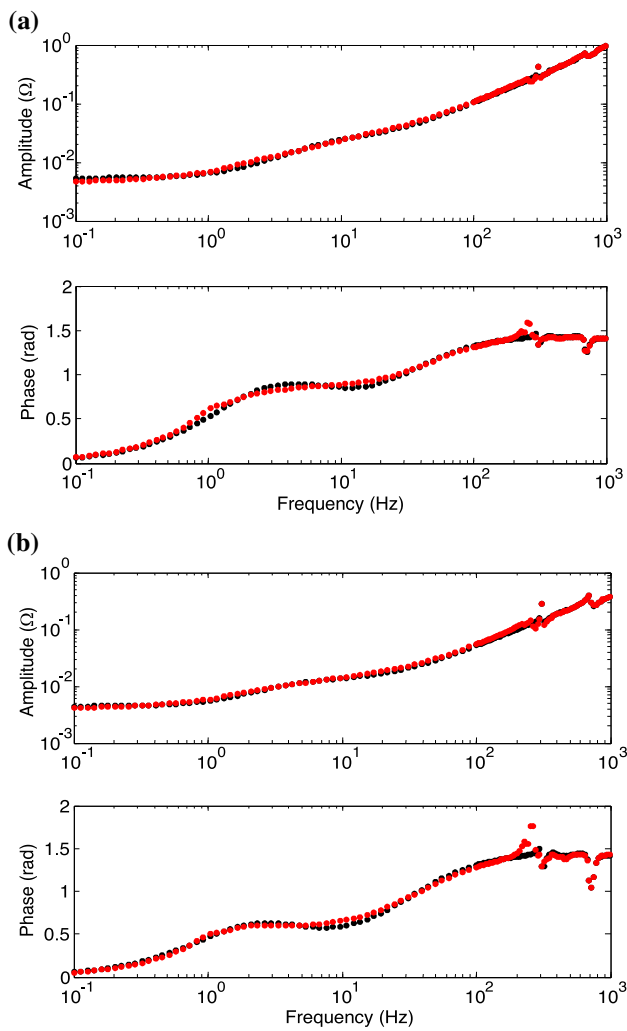


Fig. 5 **a** 1×25 and **b** 2×25 case: $T(j\omega)$ (black) and $H^*(s)$ (red) over the 0.1–1000 Hz frequency interval

conversely $T_{2 \times 25}$ is about 0.3 and 0.6 Ω again at 50 and 100 Hz. Both confirm the inductive behavior in the most relevant frequency range and their ratio is in agreement with the 1.9 screening factor commented later in Sect. 5.2.

For the 2×25 case the maximum fitting error is limited to about 3%, and it is almost double for the 1×25 case; the largest error for the 1×25 case occurs below 5 Hz and is marginal for our problem, so that we may conclude that both results are accurate to a few % at worst.

5.2 Short-circuit current

The quantities that determine the short-circuit current waveform, as calculated with the circuit of Fig. 4, are shown in Table 3 for comparison with EN 60909-0 parameters) and the waveforms are shown in Fig. 6 for the two 1×25 and 2×25 cases and two extreme values of transformer reactance

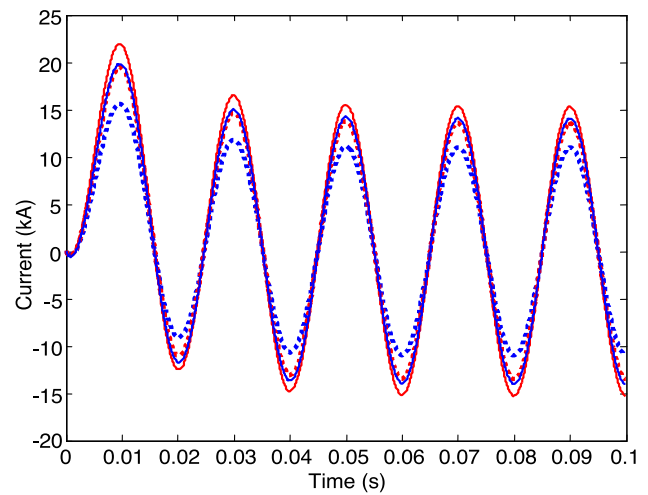


Fig. 6 Short-circuit waveforms calculated as per EN 60909-0 (ref. Table 3): solid lines ($q = 0.7$), dotted lines ($q = 0.15$), blue (case 1×25), red (case 2×25)

ratio q (whose specific value was not available for the ESS transformer).

As expected, the short-circuit current is larger for the 2×25 case since the overall impedance of the system is lower, thanks to the AT and NF combined action. The variability due to the factor q is not dramatic, limited to about 15–20%, and more evident for the 1×25 case for the same reason. The time constants shown in the last row of Table translate into a fast decay visibly lasting for one period.

The decay time constant value, when the short-circuit position is moved along the line, is more uniform for the 2×25 case, because of the mutual compensation of the parallel branch of NF, AT and remaining contact line (the first parallel branch is excluded in the 1×25 case). The same may be said for the waveform amplitude. Figure 7 reports the behavior for different position of the short-circuit event along the line, at fractional length x of 0.25, 0.5 and 0.75.

Observing the curves in Fig. 7 two elements are evident: the 2×25 case provides larger short circuit current (for the lower impedance) and there is a larger variation with respect to position x for the 1×25 case (for the exclusion of the first parallel branch, as explained above). The resulting touch voltage is calculated for the short-circuit current: For the short-circuit scenario the induced voltage waveforms of the 1×25 and 2×25 cases are shown in Fig. 8: the 1×25 induced voltage is larger despite the short-circuit current intensity in the first cycle is 15–28% larger for the 2×25 case (depending on q), thanks to the screening factor of the NF driven by the AT. A measured ratio of 1.9 may be observed, that assuming $q = 0.15$ gives exactly the observed values at the end of Table IV of [13]: for $q = 0.7$ the difference is only 12%. This validates the hypothesis of AT and NF screening for the 2×25 configuration.

Table 3 Quantities of the short-circuit waveform as in EN 60909–0

Position x	Case 1 \times 25		Case 2 \times 25	
	0.25 (3 km)		0.25 (3 km)	
React. ratio q	0.15	0.70	0.15	0.70
X/R	3.59	3.48	3.75	3.72
I_{sc} [kA]	7.77	9.94	9.58	10.81
k	1.44	1.43	1.46	1.46
I_p [kA]	15.82	20.10	19.78	22.32
I_{dc} [kA]	$10.99 e^{-t/0.0114}$	$14.06 e^{-t/0.0111}$	$13.55 e^{-t/0.0119}$	$15.29 e^{-t/0.0118}$

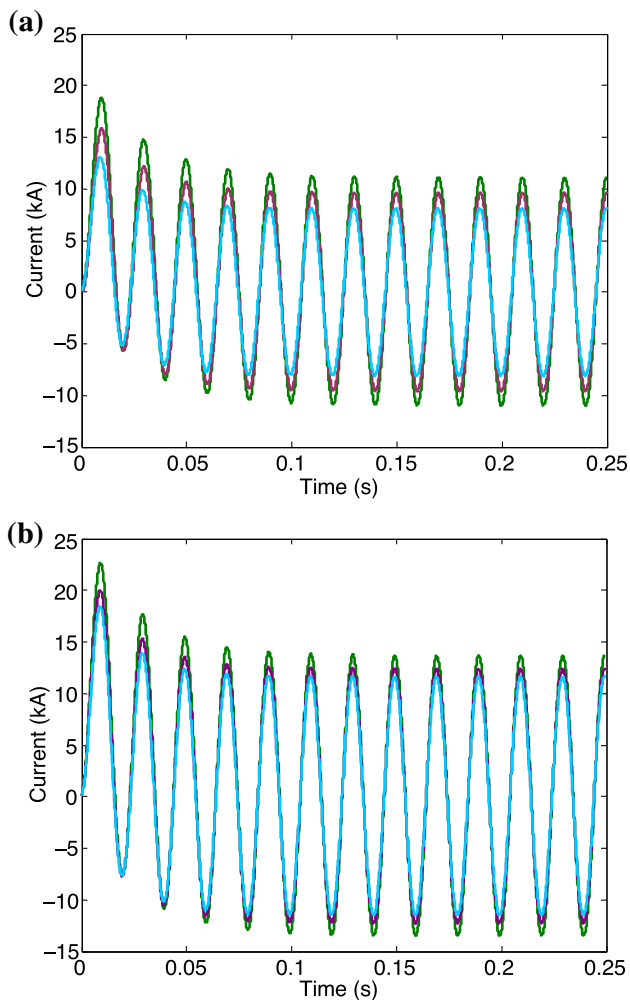


Fig. 7 Short-circuit waveforms calculated with the MTL simulator for $x = 0.25$ (light blue), $x = 0.5$ (purple) and $x = 0.75$ (green) of the line section length of 12 km: **a** 1×25 and **b** 2×25 configurations

5.3 Inrush current

Inrush current was used also for validation, so that the input comes not from the calculation in Sect. 4.2, but from measurements, as well as the induced voltage at a wayside cable was measured.

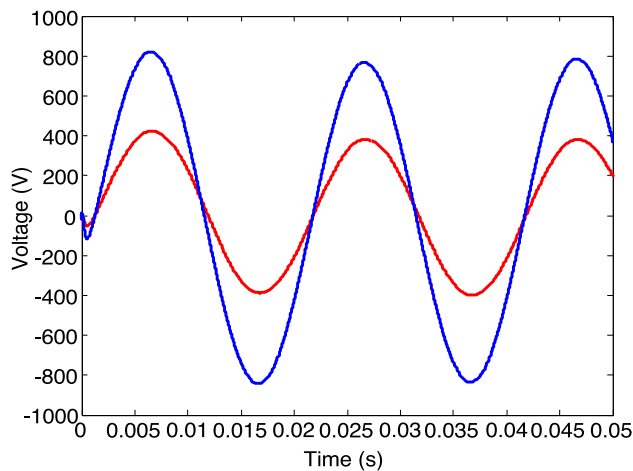


Fig. 8 Voltage induced by short circuit for 1×25 (blue) and 2×25 (red)

Table 4 Error at peak values in the 0–0.25 s interval

	Case 1 \times 25 (%)	Case 2 \times 25 (%)
Mean error in [0, 0.25s]	2.4	3.3
Maximum error in [0, 0.25s]	6.0	7.7

For the inrush current the resulting induced voltages for the 1×25 and the 2×25 cases are shown overlapped (calculation in gray, measurement in black) in Figs. 9 and 10: a slight worse accuracy can be seen for the 1×25 case, due probably to an unexpected change in the earth conductance on the day of the 1×25 test, caused by some night rain. Relative accuracy in the first 250 ms is slightly better for the 1×25 case simply because the base values are higher, that is the amount of induced voltage is larger than in the 2×25 case. Percentage error values are shown in Table 4.

It is also observed that the simulated induced voltage waveform is larger than the measured one at all points. This aspect is important when this approach is used for the demonstration of compliance to limits of electrical safety and interference in a safety-oriented perspective, thus requiring overestimation and margins.

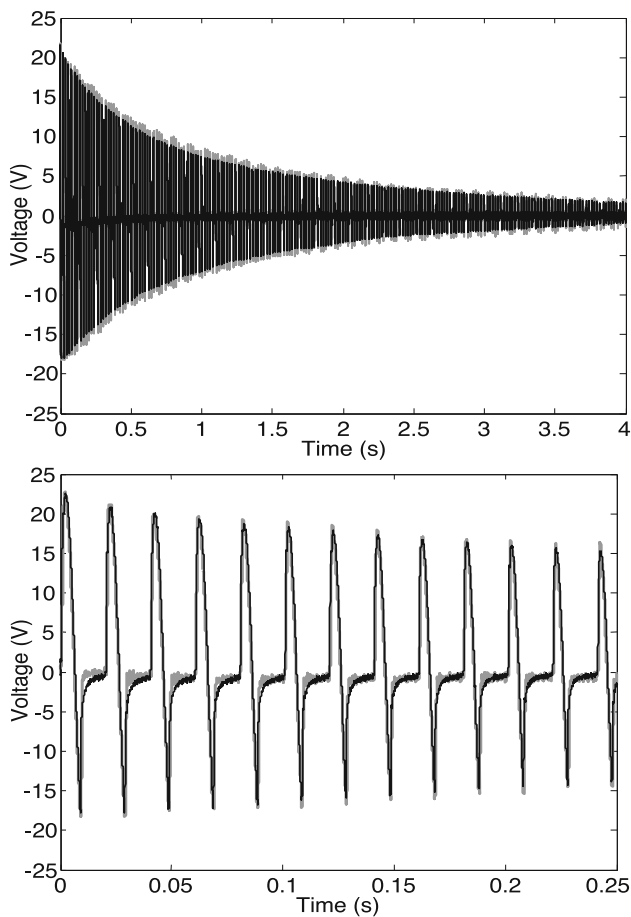


Fig. 9 Measured (black) and calculated (gray) voltage induced by inrush for the 2×25 case

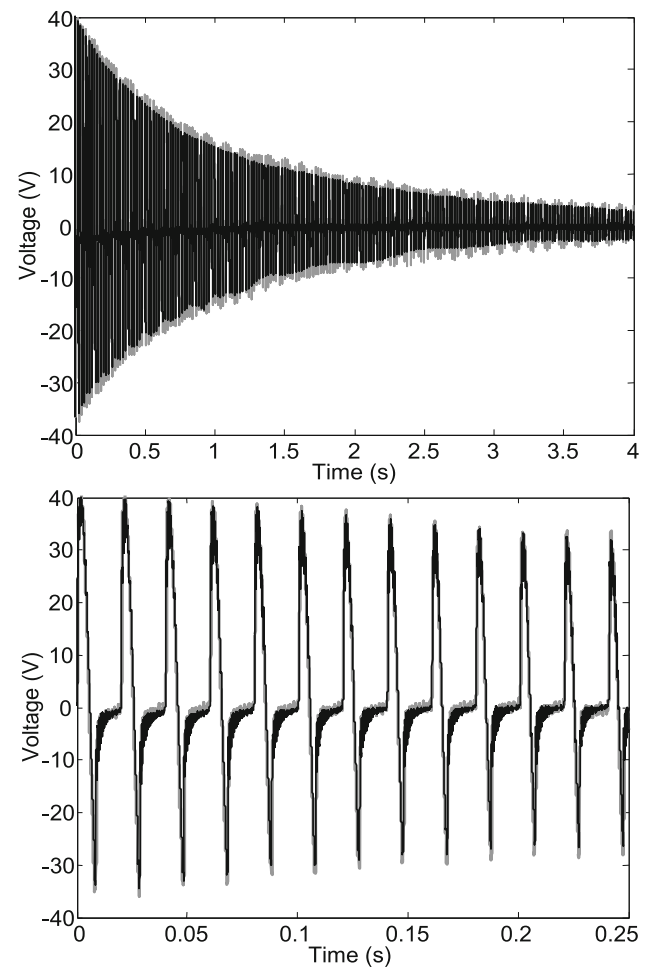


Fig. 10 Measured (black) and calculated (gray) voltage induced by inrush for the 1×25 case

6 Conclusion

This work has demonstrated the feasibility of estimation of time-domain induced phenomena for short circuit and inrush events in AC railways. The followed approach is that of selecting a source of disturbance in term of point of application (or connection in the overall system circuit) and waveform (namely the short circuit or inrush waveform, either calculated or measured). Then the method determines the transfer function in frequency domain (called “frequency response”) with respect to the output quantity (i.e., induced voltage across a victim cable of given length). Fitting the frequency response $T(j\omega)$ to a passive polynomial transfer function in the Laplace domain $H(s)$ allows estimating time-domain transients, including the frequency-domain dependency of some parameters. The frequency response may be built on simulation results (e.g., using a reliable validated simulator working in the frequency domain) or based on measurements testing an existing system with all limitations related to accessibility of worst-case scenarios).

The method solves the problem of evaluating two aspects that are not addressable with a frequency-domain approach: the peak of the induced voltage and the duration of a given voltage intensity value to compare to the duration-intensity curve of the touch voltage limits [47, 48].

The method is in principle applicable to all induction phenomena related to time domain waveforms, thus overcoming the short circuit and inrush current cases analyzed here. Alternative approaches have focused on. The study of interference to buried pipelines at the fundamental frequency depending on location and including statistical behavior [49, 50].

The method was applied to a 25 kV high-speed railway line project following the construction. Tests made on the first completed line section allowed to validate experimentally the simulated transient waveforms for inrush, that are not disruptive phenomena, compared to short circuit, and can be tested without major issues. The demonstrated accuracy for 2×25 and 1×25 configurations is in the order of few %, as shown in Table 2. It is observed that the amplitude errors are concentrated at a few half periods during the transient,

whereas the general fitting is very good. Since the objective is the assessment of compliance to electrical safety limits for humans and then those ensuring protection of equipment, the slightly overestimating results of the proposed model were welcome as a safety margin.

Further refinement is possible to improve the frequency response and achieve fitting over a more extended frequency interval. The method, however, would lose its simplicity with a limited improvement, because major transients in railways and electric networks are well described by the considered bandwidth of 1 kHz and do not need an extension to higher frequency. In addition, all measurements and parameters are characterized by an unavoidable uncertainty of some %, perfectly compatible with the observed amplitude error between simulated and measured values.

Appendix A

This Appendix contains the Matlab code for: (1) calculation of short-circuit current using the equivalent circuit of Fig. 4, (2) LMS fitting of frequency response $T(j\omega)$, and 3) determination of transient induced voltage waveform.

Short-circuit current calculation

```
%Short-circuit calculation
dt = 100e-6; T = 0.25; t = 0:dt:T - dt;
fnom = 50; phi = 0/180*pi;
EN = 27,500*1.41*sin(2*pi*fnom*t + phi);
%HV network
VN = 132,000; ANsc = 1000e+6; n = VN/27500;
XNcc = VN^2/ANsc; XNcc = XNcc/n^2;
LHVN = XNcc/(2*pi*fnom);
RHVN = 0.1*XNcc; %assumed 10%
ZHVN = [LHVN RHVN];
%ESS transformer
%name plate data:
% copper losses: 1AT = 42.3 kW, 2AT = 22.6 kW, 3AT
= 22.5 kW;
% total copper losses (19 °C) 87.5 kW, (75 °C) 106.8 kW
% total losses (75 °C) 172 kW
% Zsc = 10.53%, X/R = 10.53/0.22.
Vsec = 27,500; A1 = 60e+6; A2 = A1/2;
Xscp = 0.1053; %Referred to A1
q = 0.15; %rectance ratio
Xsc = Vsec^2/A1*Xscp;
Xd1 = 2*q/(1 + q)*Xsc;
Xd2 = 2*(1 - q)/(1 + q)*Xsc;
Xd3 = Xd2;
R11 = Vsec^2/A1*0.0025; %losses rounded to 0.5%,
0.25% pri, 0.25% sec.
R22 = Vsec^2/A2*0.00125/2;
```

```
R33 = Vsec^2/A2*0.00125/2;
RT2 = R22 + R11/2; LT2 = (Xd2 + Xd1/2)/(2*pi*fnom);
ZT2 = [LT2 RT2];
RT3 = R33 + R11/2; LT3 = (Xd3 + Xd1/2)/(2*pi*fnom);
ZT3 = [LT3 RT3];
ZT = ZT2 + ZT3;
%High-Speed traction line
x = 0.25; %Short-circuit position (x = 0...1)
LL = 12; %Length of line (km)
RCW = 0.060; %Contact + Messenger Wire: Resistance
(ohm/km)
LCW = 205e-3/314; %Contact + Messenger Wire:
Inductance (H/km)
RFEE = 0.077; %Negative Feeder: Resistance (ohm/km)
LFEE = 271e-3/314; %Negative Feeder: Inductance
(H/km)
%AutoTransformer
Vsec = 27,500; A1 = 15e + 6;
Xscp = 0.02; %Short-circuit react. with 2 windings in
parallel, ref. to A1
Xsc = Vsec^2/A1*Xscp;
RAT = Vsec^2/A1*0.01;%Losses assumed about 1%
LAT = Xsc/(2*pi*fnom);
ZAT = [LAT RAT];
cfg = 'c2 x 25'; % 'c1 x 25', 'c2 x 25'
switch cfg
case 'c1 x 25'
Zcon = ZT2 + [LCW RCW]*x*LL;
ZHSn = Zcon;
ZHSd = 1;
case 'c2 x 25'
Zcon = ZT2 + [LCW RCW]*x*LL;
Zfee = ZT3 + ([LFEE RFEE] + [LCW RCW]*(1-x))*LL
+ ZAT;
ZHSn = conv(Zcon,Zfee);
ZHSd = Zcon + Zfee;
end
ZTOTn = ZHSn + conv(ZHSd,ZHVN);
ZTOTd = ZHSd;
YTOTn = ZTOTn;
YTOTd = ZTOTd;
sys = tf(YTOTn,YTOTd);
pole(sys)
[Isct,t] = lsim(sys,EN,t);
```

LMS fitting of frequency response $T(j\omega)$

```
%H(s) fitting from T(jw), corresponding to Vcable / Isource.
%where Isource is a 1A excitation current at all frequen-
cies.
%Vcable provided as amplitude and phase.
Zsim = V(1,:).*exp(-1i*V(2,:)/180*pi);
%vector f is provided along with Vcable.
```

```

iter = 2000; tol = 1e-3;
numord = 20; denord = 10;
weight = 1./log10(f + 1);
[b,a] = invfreqs(Zsim,2*pi*f,numord,denord,weight,iter,tol);
Z = freqs(b,a,2*pi*f);
Figure (1);
subplot(2,1,1);
loglog(f,abs(Z),'k.',f,abs(Zsim),'r.');
```

ylabel('Amplitude (\Omega)');

```

subplot(2,1,2);
semilogx(f,unwrap(angle(Z)),'k.',f,angle(Zsim),'r.');
```

ylabel('Phase (rad)');

xlabel('Frequency (Hz)');

Transient induced voltage waveform

```

%Transient response calculation (example for measured
inrush)
%load inrush.mat, containing t and Iinrush (t starts from
0, otherwise t = t - t(1))
sysr = minreal(Z,1e-2);
Vinrush = lsim(sysr,Iinrush,t);
```

References

- Díaz Zayas A, García Pérez CA, Merino Gómez P (2014) Third-generation partnership project standards: for delivery of critical communications for railways. *IEEE Veh Technol Mag* 9(2):58–68. <https://doi.org/10.1109/MVT.2014.2311592>
- Ai B, Cheng X, Kürner T, Zhong Z-D, Guan K, He R-S, Xiong L, Matolak DW, Michelson DG, Briso-Rodriguez C (2014) Challenges toward wireless communications for high-speed railway. *IEEE Trans Intell Transp Syst*. <https://doi.org/10.1109/TITS.2014.2310771>
- Mariscotti A, Ruscelli M, Vanti M (2010) Modeling of audiofrequency track circuits for validation, tuning and conducted interference prediction. *IEEE Trans Intell Transp Syst* 11(1):52–60. <https://doi.org/10.1109/TITS.2009.2029393>
- Li M, Wen Y, Wang G, Zhang D, Zhang J (2020) A network-based method to analyze EMI events of on-board signaling system in railway. *Appl Sci* 10:9059. <https://doi.org/10.3390/app10249059>
- Zhao L, Li M (2012) Probability distribution modeling of the interference of the traction current in track circuits. *J Theor Appl Inf Technol* 46(1):125–131
- Mariscotti A (2021) Impact of rail impedance intrinsic variability on railway system operation, EMC and safety. *Int J Electr Comput Eng (IJECE)* 11(1):17–26. <https://doi.org/10.11591/ijece.v11i1.pp17-26>
- Havryliuk V (2018) Modelling of the return traction current harmonics distribution in rails for AC electric railway system. In: Proceedings of the 2018 international symposium on electromagnetic compatibility (EMC Europe 2018), Amsterdam, The Netherlands, August 27–30. <https://doi.org/10.1109/EMCEurope.2018.8485160>
- Ignatenko I, Tryapkin E, Vlasenko S, Onischenko A, Kovalev V (2020) Impact of return traction current harmonics on the value of the potential of the rail ground for the AC power supply system. In: VIII international scientific Siberian transport forum
- Havryliuk V, Serdyuk T (2006) Distribution of harmonics of return traction current on feeder zone and evaluation of its influence on the work of rail circuits. In: 18th International Wroclaw symposium and exhibition on electromagnetic compatibility, pp 467–470
- Yang L, Hian LC, Leong LW, Chuan Kevin OM (2018) Induced voltage study and measurement for communication system in railway. In: IEEE international symposium on electromagnetic compatibility and 2018 IEEE Asia-Pacific symposium on electromagnetic compatibility (EMC/APEMC), Suntec City, Singapore, 14–18 May. <https://doi.org/10.1109/ISEMC.2018.8393733>
- Bongiorno J, Boschetti G, Mariscotti A (2016) Low-frequency coupling: phenomena in electric transportation systems. *IEEE Electr Mag* 4(3):15–22. <https://doi.org/10.1109/MELE.2016.2584959>
- Mariscotti A (2012) Results on the power quality of French and Italian 2x25 kV 50 Hz railways. In: International instrumentation and measurement technology conference, I2MTC, Graz, Austria, May 13–16. <https://doi.org/10.1109/I2MTC.2012.6229341>
- Mariscotti A (2011) Induced voltage calculation in electric traction systems: simplified methods, screening factors and accuracy. *IEEE Trans Intell Transp Syst* 12(1):201–210. <https://doi.org/10.1109/TITS.2010.2076327>
- Bongiorno J, Mariscotti A (2014) Experimental validation of the electric network model of the Italian 2x25 kV 50 Hz railway. In: 20th IMEKO TC4 symposium on measurements of electrical quantities, Sept 15–17, 2014, Benevento, IT, pp 964–970
- Garg R, Mahajan P, Kumar P (2014) Sensitivity analysis of characteristic parameters of railway electric traction system. *Int J Electron Electr Eng*. <https://doi.org/10.12720/ijeee.2.1.8-14>
- Zhai Y, Wu M (2022) Analysis on the 2x25-kV 50 Hz traction power supply system: short-circuit modeling. In: 5th international conference on electrical engineering and information technologies for rail transportation (EITRT), 21–23 Oct 2021, Beijing, China. https://doi.org/10.1007/978-981-16-9905-4_59
- Battistelli L, Pagano M, Proto D (2011) 2x25-kV 50 Hz high-speed traction power system: short-circuit modeling. *IEEE Trans Power Deliv* 26(3):1459–1466. <https://doi.org/10.1109/TPWRD.2010.2100832>
- Huh J-S, Kang B-W, Shin H-S, Kim J-C (2010) A study on the reduction of onboard transformer inrush current of electric railway. *Trans Korean Inst Electr Eng* 59(12):2125–2130
- Li Z, Jia Z, Xi K, Chen Y (2019) Mechanism analysis of sympathetic inrush in traction network cascaded transformers based on flux-current circuit model. *Energies* 12(21):4210. <https://doi.org/10.3390/en12214210>
- D'Antona G, Brenna M, Manta N (2012) Modeling and measurement of the voltage transients at the phase to phase changeover section of the Italian High Speed Railway System. In: IEEE international workshop on applied measurements for power systems (AMPS), 26–28 Sept, Aachen, Germany. <https://doi.org/10.1109/AMPS.2012.6344006>
- Seferi Y, Clarkson P, Blair SM, Mariscotti A, Stewart BG (2019) Power quality event analysis in 25 kV 50 Hz AC railway system networks. In: IEEE international workshop on applied measurements for power systems, Sept 25–27, Aachen, Germany. <https://doi.org/10.1109/AMPS.2019.8897765>
- Zhang Z, Zhang Z, Li K, Hao R, You X, Zheng TQ (2021) An uninterruptible smart electric neutral section executor for AC electrified railway. In: 2021 IEEE 12th energy conversion congress & exposition-Asia (ECCE-Asia), 24–27 May, Singapore. <https://doi.org/10.1109/ECCE-Asia49820.2021.9479062>
- Li T, Wu G, Zhou L, Gao G, Wang W, Wang B, Liu D, Li D (2011) Pantograph arcing's impact on locomotive equipments. In: IEEE 57th Holm conference on electrical contacts (Holm), 11–14 Sept 2011, Minneapolis, MN, USA. <https://doi.org/10.1109/HOLM.2011.6034812>

24. Wu G, Wu J, Wei W, Zhou Y, Yang Z, Gao G (2018) Characteristics of the sliding electric contact of pantograph/contact wire systems in electric railways. *Energies* 11:17. <https://doi.org/10.3390/en11010017>
25. Crotti G et al (2018) Pantograph-to-OHL arc: conducted effects in DC railway supply system. In: IEEE 9th international workshop on applied measurements for power systems (AMPS), Bologna, Italy, Sept 26–28. <https://doi.org/10.1109/AMPS.2018.8494897>
26. Mariscotti A, Giordano D (2020) Experimental characterization of pantograph arcs and transient conducted phenomena in DC railways. *Acta Imeko* 9(2):10–17. https://doi.org/10.21014/acta_imeko.v9i2.761
27. Mariscotti A, Giordano D, Delle Femine A, Signorino D (2020) Filter transients onboard DC rolling stock and exploitation for the estimate of the line impedance. In: Proceedings of the international instrumentation and measurement technology conference, Dubrovnik, Croatia, May 25–28. <https://doi.org/10.1109/I2MTC43012.2020.9128903>
28. Gu J, Yang X, Zheng TQ, Wang M (2018) Fault analysis of traction power system in urban rail transit. In: IEEE international power electronics and application conference and exposition (PEAC), Shenzhen, China, 4–7 Nov. <https://doi.org/10.1109/PEAC.2018.8590638>
29. Chen TH, Liao RN (2016) Modelling, simulation, and verification for detailed short-circuit analysis of a 1×25 kV railway traction system. *IET Gener Transm Distrib* 10(5):1124–1135. <https://doi.org/10.1049/iet-gtd.2015.0501>
30. Mariscotti A, Pozzobon P (2000) Measurement of the internal impedance of traction rails at 50 Hz. *IEEE Trans Instrum Meas* 49(2):294–299. <https://doi.org/10.1109/19.843067>
31. Zhu F, Li P, Li J, Li X, Shen D (2016) Calculation of rail internal inductance and analysis of its influence factors. *Zhongguo Tiedao Kexue/China Railw Sci* 37(5):108–113. <https://doi.org/10.3969/j.issn.1001-4632.2016.05.15>
32. Zhu F, Li P, Li J, Li X, Liu Z (2017) Calculation of alternating-current impedance for the rail of electric railway. *Zhongguo Tiedao Kexue/China Railw Sci* 39(12):38–42. <https://doi.org/10.3969/j.issn.1001-8360.2017.12.006>
33. Mirzaei M, Ripka P (2018) Analysis of material effect on rail impedance. In: International universities power engineering conference (UPEC), Glasgow, UK, 4–7 Sept. <https://doi.org/10.1109/UPEC.2018.8541860>
34. Mariscotti A, Pozzobon P (2005) Experimental results on low rail-to-rail conductance values. *IEEE Trans Veh Technol* 54(3):1219–1222. <https://doi.org/10.1109/TVT.2005.844667>
35. Lucca G (2017) Railway track transmission line model: calculation of rail conductance by means of boundary element method. *IET Sci Meas Technol* 11(8):976–982. <https://doi.org/10.1049/iet-smt.2017.0165>
36. Bongiorno J, Mariscotti A (2015) Evaluation of performances of indexes used for validation of simulation models based on real cases. *Int J Math Models Methods Appl Sci* 9:29–43
37. Mariscotti A, Pozzobon P, Vanti M (2007) Simplified modelling of 2x25 kV AT railway system for the solution of low frequency and large scale problems. *IEEE Trans Power Deliv* 22(1):296–301. <https://doi.org/10.1109/TPWRD.2006.883020>
38. Pilo E, Rouco L, Fernandez A (2003) A reduced representation of 2x25kV electrical systems for high-speed railways. In: 2003 IEEE/ASME joint rail conference, Apr 22–24, Chicago, IL, USA, pp 199–205. <https://doi.org/10.1109/RRCON.2003.1204665>
39. Cella R, Giangaspero G, Mariscotti A, Montepagano A, Pozzobon P, Ruscelli M, Vanti M (2006) Measurement of AT electric railway system currents and validation of a multiconductor transmission line model. *IEEE Trans Power Deliv* 21(3):1721–1726. <https://doi.org/10.1109/TPWRD.2006.874109>
40. Gustavsen B, Semlyen A (1999) Rational approximation of frequency domain responses by vector fitting. *IEEE Trans Power Deliv* 14(3):1052–1061. <https://doi.org/10.1109/61.772353>
41. Ubolli A, Gustavsen B (2011) Comparison of methods for rational approximation of simulated time-domain responses: ARMA, ZD-VF, and TD-VF. *IEEE Trans Power Deliv* 26(1):279–288. <https://doi.org/10.1109/TPWRD.2010.2080361>
42. CENELEC EN 60909-0 (2001) Short-circuit currents in three-phase ac systems—part 0: calculation of currents
43. Pozzobon P (1998) Transient and steady-state short-circuit currents in rectifiers for DC traction supply. *IEEE Trans Veh Technol* 47(4):1390–1404. <https://doi.org/10.1109/25.728534>
44. Chiesa N (2010) Power transformer modeling for inrush current calculation. Dissertation, Norwegian University of Science and Technology
45. Altun H, Sünter S, Aydoğmuş Ö (2021) Modeling and analysis of a single-phase core-type transformer under inrush current and nonlinear load conditions. *Electr Eng* 103:2961–2972. <https://doi.org/10.1007/s00202-021-01283-9>
46. Waindok A (2012) A method for calculation of the inrush current in single phase transformer including the residual flux. *Przeegląd Elektrotechniczny* 05b:194–201
47. IEC 62128-1 (2011) Railway applications—fixed installations—electrical safety, earthing and the return circuit—part 1: protective provisions against electric shock
48. ITU-T K.68 (2008) Operator responsibilities in the management of electromagnetic interference by power systems on telecommunication systems
49. Lucca G (2011) Two steps numerical method for calculating the AC interference from a faulty power line on nearby buried pipelines. *Euro Trans Electr Power* 21:2037–2052. <https://doi.org/10.1002/etep.557>
50. Czarnywojtek P, Machczynski W (2018) Wave propagation effects induced in transmission pipelines by EMI from power lines. *Electr Eng* 100:1739–1747. <https://doi.org/10.1007/s00202-017-0646-8>

Publisher's Note Springer Nature remains neutral with regard to jurisdictional claims in published maps and institutional affiliations.

Springer Nature or its licensor holds exclusive rights to this article under a publishing agreement with the author(s) or other rightsholder(s); author self-archiving of the accepted manuscript version of this article is solely governed by the terms of such publishing agreement and applicable law.